JACS Au
AN OPEN ACCESS JOURNAL OF THE AMERICAN CHEMICAL SOCIETY

pubs.acs.org/jacsau
Article

How the Larger Methionine-Rich Domain of CueO from *Hafnia alvei* Enhances Cuprous Oxidation

Umberto Contaldo,* Paolo Santucci, Alexandra Vergnes, Philippe Leone, Jérôme Becam, Frédéric Biaso, Marianne Ilbert, Benjamin Ezraty, Elisabeth Lojou,* and Ievgen Mazurenko*

Cite This: *JACS Au* 2025, 5, 1833−1844
Read Online

ACCESS | Metrics & More | Article Recommendations | Supporting Information

ABSTRACT: CueOs, members of the multicopper oxidase family, play a crucial role in bacterial copper detoxification. These enzymes feature a unique methionine-rich (Met-rich) domain, which is essential for the oxidation of Cu^+ to Cu^{2+}. Recent studies using CueO from *Escherichia coli* (*Ec*CueO) suggest that the Met-rich domain facilitates Cu^+ recruitment from highly chelated species. To further explore this hypothesis, we produced and characterized a novel CueO from the bacterium *Hafnia alvei* (*Ha*CueO). *Ha*CueO possesses a significantly larger Met-rich domain than *Ec*CueO, providing new insights into the role of this domain in cuprous oxidase activity. We first showed that *Ha*CueO was as efficient in copper detoxification as *Ec*CueO in vivo. The structures of both wild-type *Ha*CueO and a variant lacking the Met-rich domain were resolved by X-ray crystallography and simulated by molecular dynamics, offering a detailed structural basis for understanding their functions. Cuprous oxidase activity was then quantified either from free electrogenerated Cu^+ with CueO immobilized on an electrode or from different Cu^+-complexes with CueO in solution. These methods enabled the fine-tuning of Cu^+ chelation strength. Consistent with findings for *Ec*CueO, it was confirmed that the Met-rich domain of *Ha*CueO is dispensable for Cu^+ oxidation when weakly chelated Cu^+ is used. However, its role becomes crucial as chelation strength increases. Comparative analyses of cuprous oxidase activity between *Ha*CueO and *Ec*CueO revealed that *Ha*CueO outperforms *Ec*CueO, demonstrating superior efficiency in oxidizing Cu^+ from chelated forms. This enhanced activity correlates with the higher methionine content in *Ha*CueO, which appears to play a pivotal role in facilitating Cu^+ oxidation under conditions of stronger chelation.

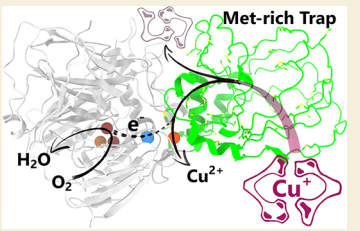

KEYWORDS: *multicopper oxidase, CueO, Cu^+ oxidation, copper homeostasis, methionine-rich domain, electrochemistry, MCO structure*

INTRODUCTION

Copper is an essential element for microorganisms and can serve as a cofactor in metalloenzymes. However, high concentrations of copper are toxic to cells.[1] Copper toxicity is observed under both aerobic and anaerobic conditions, with aerobic toxicity primarily linked to the generation of reactive oxygen species (ROS) through the Fenton reaction. Under anoxic conditions, cuprous ions (Cu^+) predominate and their toxicity involves mismetalation and protein aggregation.[1,2] To cope with Cu-mediated toxicity, microorganisms have adapted copper homeostasis systems. In Gram-negative bacteria such as *Escherichia coli*, at least three systems are involved: (I) CusCFBA, an efflux pump responsible for the translocation of copper to the extracellular environment; (II) CopA, a P-type ATPase that pumps copper from the cytoplasm to the periplasm; and (III) CueO, a periplasmic multicopper oxidase (MCO) that catalyzes the oxidation of Cu^+ to less toxic Cu^{2+}, limiting therefore ROS production. So far, three crystal structures of CueOs from Gram-negative bacteria have been solved: *E. coli* (*Ec*CueO), *Ochrobactrum* sp. (*Oc*CueO), and *Thermus thermophilus* HB27 (*Tt*CueO). Their overall structure shows a conserved architecture consisting of three β-barrel type domains, similar to the structures of other MCOs such as laccase, bilirubin oxidase, and ascorbate oxidase. This allows for the coordination of four copper atoms organized into two main active centers: the mononuclear Cu-T1 and a trinuclear cluster (TNC) composed of one Cu-T2 and two Cu-T3. The Cu-T1 catalyzes the oxidation of various substrates and transfers electrons to the TNC, which catalyzes the four-electron reduction of oxygen to water.

The CueO structure is characterized by an additional domain rich in methionine residues (Met-rich) that surrounds the Cu-T1 center, making it buried and less accessible to solvents (Figure 1A). A fifth copper (Cu5) coordinated at the interface between domain III and the Met-rich domain was revealed in the crystal structure of the Cu-T1-depleted *Ec*CueO, solved in the presence of an excess of substrate Cu^+ (Figure 1B).[3] The presence of the Met-rich domain in the CueO enzyme affects enzymatic activity in different manners. First, lower catalytic performances for phenolic substrates compared to fungal laccases are observed, consistently

Received: January 20, 2025
Revised: March 31, 2025
Accepted: March 31, 2025
Published: April 10, 2025

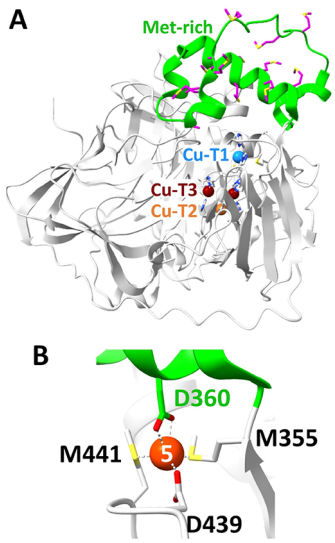

Figure 1. (A) Ribbon diagram of *Ec*CueO X-ray structure (PDB entry: 3OD3). The Met-rich domain is highlighted in lime green and Met residues in magenta. Copper atoms are represented as colored spheres, Cu-T1, Cu-T2, and Cu-T3, respectively, colored in cyan, brown, and dark red. (B) Cu5 coordination between the domain III and the Met-rich domain observed in the catalytically inactive *Ec*CueO ΔCu-T1 variant (PDB entry: 3NT0); it represents the substrate Cu^{+} docked to the cuprous oxidase active site. In *Ec*CueO, Cu5 is coordinated by M355, M441, D439, and D360.

enhanced in the *Ec*CueO variant lacking the Met-rich domain (ΔMet).[4,5] Second, the addition of Cu^{2+} ions restores the phenol oxidase activity of CueOs in solution, because their subsequent coordination at the Cu5 center offers an electron transfer pathway.[4,6−8] On the other hand, Cu^{+} ions can also bind to the Cu5 site with consequent rapid oxidation to the less toxic Cu^{2+} coupled to O_2 reduction. We have recently shown that the Met-rich domain of *Ec*CueO is dispensable for the oxidation of weakly chelated Cu^{+} ions.[9] However, we further demonstrated that the structural organization of multiple solvent-accessible methionine residues in the Met-rich domain facilitates the recruitment of strongly chelated Cu^{+} ions in vitro. Consistently, the loss of the Met-rich domain affected the viability of *E. coli* cells in vivo in the presence of toxic copper levels.

The bacterial CueO superfamily comprises 4859 known protein sequences belonging to 14 homologous families.[10] Depending on the microorganism, the Met-rich domain is highly diverse in terms of the number and nature of its amino acids, especially methionine.[11,12] To validate the previously proposed role of the Met-rich domain, we provide here the biochemical, structural, spectroscopic, and catalytic characterization of a novel CueO from the Gram-negative bacteria *Hafnia alvei* (*Ha*CueO). Structural analysis of *Ha*CueO reveals a conserved architecture similar to other CueOs in terms of protein backbone, copper centers (Cu-T1 and TNC), and residues of the Cu5 binding site. The key difference between *Ec*CueO and *Ha*CueO lies in the Met-rich domain size and composition. We especially discuss how the presence of a larger Met-rich domain impacts the catalytic performances of *Ha*CueO for cuprous oxidation compared to *Ec*CueO.

RESULTS AND DISCUSSION

Hafnia alvei CueO Detoxifies the Periplasm of *E. coli* Cells

We selected the *Ha*CueO sequence from the Uniprot database (reference A0A377PPH3) based on its high residue conservation compared to *Ec*CueO (Figure S1). The BLAST alignment of the two sequences reveals 67% protein identity, which increases to 70% when the sequences without Met-rich domains are aligned. The most notable difference lies in the Met-rich domain, with *Ha*CueO containing 22 additional residues, including 6 more methionines (Figure 2A). Two

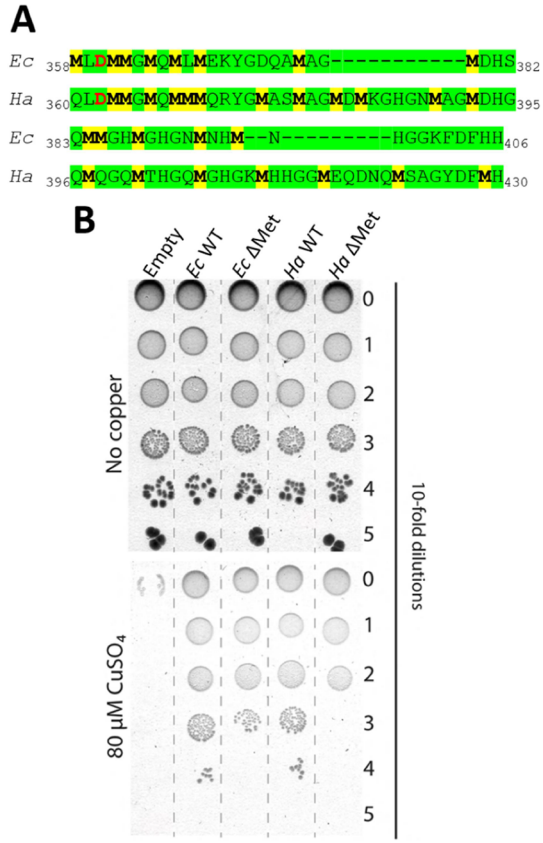

Figure 2. (A) Met-rich domain sequences alignment of *Ec*CueO (*Ec*) and *Ha*CueO (*Ha*). The methionine residues are highlighted in yellow and bold, while the aspartate Cu5 ligand from the Met-rich domain is highlighted in bold red: D360 and D362 for *Ec* and *Ha*, respectively. The number of methionine residues is 13 for *Ec*CueO and 19 for *Ha*CueO. (B) Effect of copper stress on *E. coli* cell viability. Cells have been deleted of native *cueO* and *cusB* genes, in order to increase the strain's copper sensitivity, and trans-complemented with the CueO vectors.

types of constructs were built by using the native gene of *Ha*CueO, yielding the WT enzyme, and a truncated variant where the entire Met-rich domain is absent, yielding the ΔMet enzyme. To investigate the cuproxidase activity of *Ha*CueO enzyme under physiologic conditions, we used a trans-complementation test previously developed.[9] In this assay, a copper-sensitive *E. coli* Δ*cusB* Δ*cueO* strain was transformed with plasmids carrying genes encoding for *Ec*CueO, *Ha*CueO, their ΔMet mutants, or an empty plasmid as a control (Tables S1 and S2).

All variants were able to complement the Δ*cusB* Δ*cueO* strain, conferring some copper resistance (Figure 2B). The

https://doi.org/10.1021/jacsau.5c00076
JACS Au 2025, 5, 1833−1844

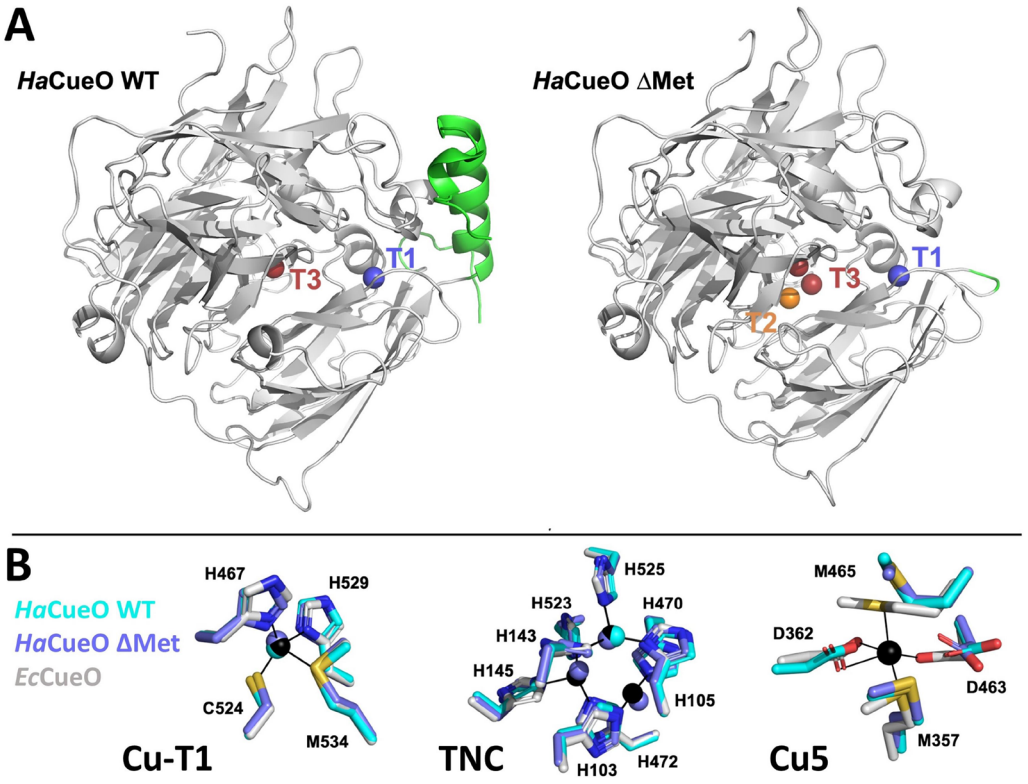

Figure 3. Crystal structure of *Ha*CueO: a typical CueO fold with conserved copper centers. (A) Ribbon diagram of *Ha*CueO WT (8R4F), with the partial Met-rich domain in *Ha*CueO WT and the substituting GG linker in *Ha*CueO ΔMet highlighted in lime green. Copper atoms are shown as colored spheres: Cu-T1 in blue, Cu-T2 in brown, and Cu-T3 in dark red. (B) Superposition of *Ha*CueO WT (in cyan) ΔMet (in violet) with *Ec*CueO (in light gray) at the Cu-T1, TNC, and Cu5 copper centers. Black lines correspond to copper coordination by *Ec*CueO residues. *Ec*CueO PDB entries 1KV7 and 3NT0 were used for superposition at the Cu-T1 and TNC centers and at the Cu5 center, respectively. For clarity purposes, only the *Ha*CueO residues are labeled, and different orientations were chosen for the three copper centers.

highest resistance was observed with the two WT enzymes, indicating that heterologous *Ha*CueO can protect *E. coli* cells against copper stress. The two ΔMet variants were less effective, although their resistance remained significantly higher than that of the empty plasmid control, in agreement with our previous observation.[9] However, the fact that *Ha*CueO exhibits detoxification efficiency equal to that of *Ec*CueO, despite possessing a more extensive Met-rich domain, was puzzling. Therefore, we decided to purify and characterize *Ha*CueO in vitro to better understand the role of this larger Met-rich domain on the enzyme activity.

Biochemical and Spectroscopic Characterizations of *Ha*CueOs

The expression and isolation of pure and homogeneous monomeric *Ha*CueO proteins have been performed as previously reported (Figure S2).[9] Both *Ha*CueO preparations show a blue coloration, indicating the presence of the Cu-T1 center. In the UV−visible absorption spectra (Figure S3), a peak at 610 nm is observed, corresponding to Cu-T1, along with a shoulder at 330 nm attributed to the presence of Cu-T3. EPR spectroscopy confirms the integrity of the Cu clusters. All the isolated *Ha*CueOs in MOPS buffer exhibit characteristic signals corresponding to Cu-T1 and Cu-T2 signatures (Figure S4). The Cu-T1 presents a near-axial signal with $g_{\|} = 2.24$, $g_{\perp} = 2.04$ and $A_{\|}(Cu) = 62 \times 10^{-4}$ cm^{-1}, whereas the Cu-T2 site is characterized by $g_{\|} = 2.25$ and $A_{\|}(Cu) = 180 \times 10^{-4}$ cm^{-1}. These values are very close to those previously reported for *Ec*CueO,[9] indicating a high degree of structural and geometrical conservation of the Cu-T1 and Cu-T2 sites within these enzymes. An additional signal ($g_{\|} = 2.21$ and $A_{\|}(Cu) = 159 \times 10^{-4}$ cm^{-1}) is present as previously detected in all *Ec*CueO variants and is probably linked to a copper site located at the protein surface.[9] Copper content determination by ICP-OES (Table S3) indicates that the two *Ha*CueOs have on average less than four coppers per protein, suggesting that not all enzymatic preparations are fully metalated. This is consistent with the EPR quantification and absorbance values at 610 and 330 nm (Table S3), which suggest that nonmetalation mainly concerns the TNC. Such incomplete metalation after purification is often observed for CueOs and, more generally, for MCO enzymes. However, it has been shown that even apo-enzymes can be rapidly and fully metalated in vitro by the addition of Cu^{2+} or, more efficiently, Cu^{+}.[13,14] Since all our activity assays contain an excess of copper species as substrates, rapid metalation occurs for all enzymes at the initial phase of the assay, enabling a reliable comparison of their activities.

Structural Characterization of WT and ΔMet *Ha*CueOs

The circular dichroism spectra of *Ha*CueO WT and ΔMet preparations do not show major differences, underlining that partial deletion of the Met-rich domain does not affect the secondary structure (Figure S5). In order to get more insight about any structural differences, we solved the X-ray crystal structures of *Ha*CueOs WT and ΔMet (PDB entries 8R4F and 8R4H, respectively) at 3.2 and 3.0 Å, respectively (Figure 3 and Table S4).

*Ha*CueO WT crystallized in the space group $P2_12_12_1$ with five identical molecules in the asymmetric unit with root-mean-

https://doi.org/10.1021/jacsau.5c00076
JACS Au 2025, 5, 1833−1844

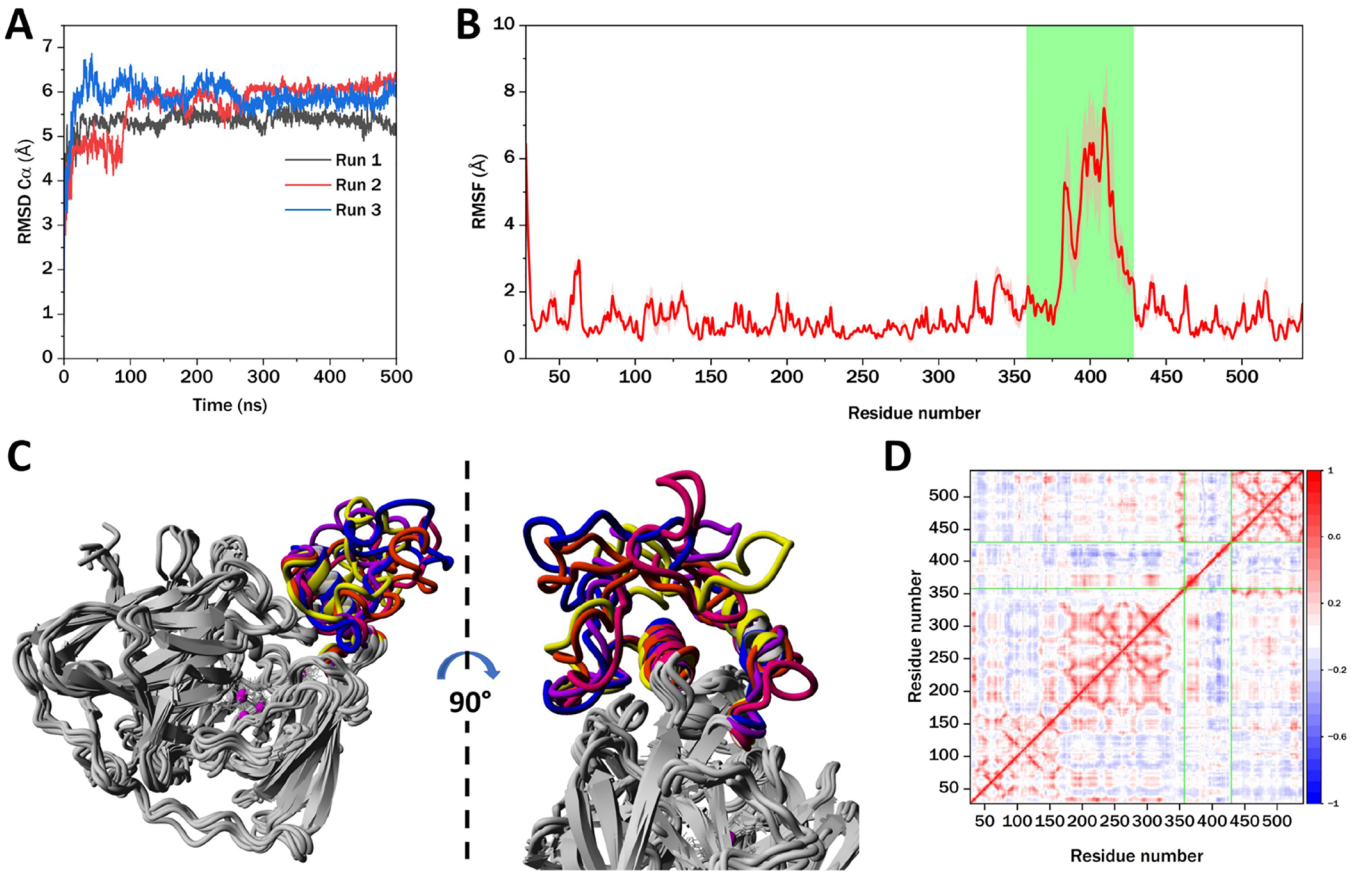

Figure 4. Analysis of three parallel runs of 500 ns MD simulation of *Ha*CueO. (A) RMSD of Cα from the starting structure. (B) Average RMSF of each residue of *Ha*CueO. Pale-red curve envelope corresponds to the standard deviation (SD). Lime-green shaded zone indicates the Met-rich domain. (C) Superimposed representative conformations of *Ha*CueO obtained after clustering of an individual MD-trajectory with RMSD threshold 3 Å. The Met-rich domain is colored according to the conformations, the rest of the protein is gray. (D) Dynamic cross-correlation matrix of *Ha*CueO residues movement. Color coding: from −1 (fully anticorrelated movement) to +1 (fully correlated movement). The borders of the Met-rich domains are indicated with lime-green lines.

square deviation (RMSD) of ∼0.23 Å. The *Ha*CueO WT structure displays the typical fold of CueO with three similar azurin-like β-sandwich domains. Furthermore, the Cu-T1, TNC, and Cu5 centers are strictly conserved (Figure 3B). However, while a copper ion is present in the Cu-T1 center, no ion occupies the Cu5 center, and only one Cu-T3 ion is present in the TNC site. Such depletion of the TNC center was previously observed in the *Ec*CueO and *Oc*CueO structures.[13,15] This phenomenon could be due to X-ray-induced radiation damage or to aerobically grown crystals. As observed in previous cuproxidase structures,[15−17] part of the Met-rich domain could not be modeled, except residues 359−382 comprising the α-helix lying near the Cu-T1 center and participating to the Cu5 center, and residues 423−430. Actually, the remaining part of the Met-rich domain (residues 383−422) corresponds to a probably intrinsically disordered loop that is 22 residues shorter in *Ec*CueO, which could be modeled in only one structure, despite a weak electron density map, thanks to crystal packing constraints.[3]

*Ha*CueO ΔMet crystallized in the H3 space group with two identical molecules in the asymmetric unit (RMSD ∼ 0.15 Å). In this construct, designed accordingly to the truncated mutant of *Ec*CueO,[4] the Met-rich domain (residues 359−430) was replaced by a Gly-Gly linker to not deform the CueO scaffold. Indeed, *Ha*CueO WT and ΔMet structures are identical (RMSD ∼ 0.44 Å). Consequently, the T1 and TNC centers are conserved in the *Ha*CueO ΔMet structure (Figure 3B): one ion is present in the T1 center, and three ions are present in the TNC center, with the Cu-T2 having an occupancy of 0.5.

Molecular Dynamics of the Met-Rich Domain

Since the Met-rich domain is disordered and we were unable to fully resolve its structure, we performed a MD simulation of the *Ha*CueO WT, using the structure predicted by AlphaFold 3 as a starting point (Figure S6). Three parallel runs of 500 ns each, with different random seeds, were conducted. All three runs showed a consistent trend of rapid partial folding of the Met-rich domain early in the simulation from the unnatural open loop of the AlphaFold 3 starting structure (Figure 4 and Movie S1). As a result, the RMSD of Cα atoms from the starting structure increased rapidly to 5−6 Å within the first 10 ns and then remained stable for the rest of the simulation (Figure 4A). Overall, the time-averaged structures obtained from the MD simulations correspond well to the resolved part of the crystal structure, with the RMSD between Cα atoms of residues common to both the crystallographic and simulated structures being 4.27 ± 0.05 Å (Figure S7).

As expected, the Met-rich domain appears to be the most flexible part of the protein, as shown by root-mean-square fluctuation (RMSF) values reaching 7−8 Å for the residues in the middle of the domain. In contrast, the large α-helix at the

https://doi.org/10.1021/jacsau.5c00076
JACS Au 2025, 5, 1833−1844

beginning of the domain (residues P359−Y373) is much less flexible, with RMSF values not exceeding 2 Å for its residues (Figure 4B). Clustering of multiple conformations observed reveals that, while this helix remains stable throughout the simulation, the rest of the domain is largely disordered and fluctuates significantly around it (Figures 4C, S8, and Movie S1). Comparison with the simulation of *Ec*CueO performed under the same conditions shows a similar RMSF profile, except that the most flexible residues of *Ec*CueO Met-rich domain fluctuate less, with a maximum RMSF of 4−5 Å (Figures S9 and S10).

The dynamic cross-correlation matrix (DCCM) of *Ha*CueO captures the correlated movements of the residues. Three β-barrel domains of the protein are easily recognizable on the DCCM matrix as three square, well-correlated patterns (Figure 4D). Most of the Met-rich domain appears to be weakly anticorrelated or not correlated at all with the rest of the protein, confirming its flexible disordered nature. The only exception is the large α-helix, which seems to be correlated and moves together with several residues from the second β-barrel domain. Interestingly, while the DCCM of *Ec*CueO exhibits a similar pattern, its α-helix does not display the same correlation with the second domain (Figure S9). This suggests that, in *Ha*CueO, the α-helix interacts more strongly with the rest of the protein compared to *Ec*CueO.

Moreover, all three simulation runs show a tendency for the formation of an additional helix composed of the residues G415−G425 in (Figure S11). Notably, the majority of these residues do not have counterparts in the *Ec*CueO sequence (Figure S10), suggesting that this helix might be unique to *Ha*CueO. Another small helix is observed at the end of the domain between D427 and H430, and a few transient helices emerge between G374 and G404, though these do not form dominant secondary structures over the time scale of the simulation.

Principal component analysis (PCA) was performed on *Ha*CueO trajectories to capture the most dominant collective residue motions (Figure S12). Three first principal components were analyzed in more detail (Figure S13 and Movie S2). In all three simulations, these components represent the movements of the flexible residues of the Met-rich domain, although the trajectories of these movements are different in parallel simulations. Two first principal components are usually well intercorrelated between themselves forming several conformation clusters with more or less expanded Met-rich domain, as attested by the variation of the protein gyration radius within these clusters (Figure S13).

In conclusion, MD results allow defining two distinct regions in the Met-rich domain of *Ha*CueO: (a) a large α-helix at the beginning that remains mostly stable throughout the simulations due to its secondary structure and interactions with the second β-barrel domain and (b) a flexible region encompassing the rest of the domain, which fluctuates around the α-helix without adopting well-defined conformations. Compared to *Ec*CueO, the higher flexibility of this region, along with the larger radius of gyration and increased solvent-accessible surface area of *Ha*CueO (Figure S10), might influence the probability of substrate encounter and its binding mode. Additionally, the simulations suggest a second large α-helix of ca. 10 residues likely to be formed at the end of the Met-rich domain. However, since this helix is unresolved in the crystallographic structure, its stability is likely moderate, unless it is stabilized through interactions with the substrate or protein partners.

Electrochemical Cuprous Oxidase Activity of CueOs

We recently employed electrochemical tools to measure and quantify the cuprous oxidase activity of CueOs immobilized at carbon nanotube (CNT)-based electrodes.[8,9] We proved that enzymatic cuprous oxidation can be detected by orienting the CueO at the electrode surface in a manner that impedes most of the electron transfer between the CNT surface and the first electron acceptor (Cu-T1). The substrate is provided in an unchelated Cu^{2+} form, and by applying a sufficiently reductive potential, Cu^{2+} is reduced to Cu^{+} at the CNT surface, near the adsorbed enzyme. The electro-generated Cu^{+} then binds at the Cu5-site, where it is oxidized, transferring electrons to the Cu-T1 and subsequently to the TNC. The resulting Cu^{2+} is released, completing the catalytic cycle and leading to an increase in the catalytic reduction current. Earlier, we confirmed this mechanism by constructing ΔCu5 and ΔCu-T1 mutants of *Ec*CueO. Indeed, both lost their cuprous oxidation ability.[9] We hereby studied the electrocuprous oxidase activity of *Ha*CueO under the same conditions as those used for *Ec*CueO.

To investigate the electrocuprous oxidase activity of *Ha*CueO, the initial step is to ascertain its orientation on electrochemical interfaces. For that purpose, we tuned the electrode surface chemistry by deposits of thin films of either positively or negatively charged CNTs. Similar to *Tt*CueO and *Ec*CueO,[8,9] *Ha*CueO shows a preferential orientation on positively charged CNTs and displays lower direct electron transfer (DET) current on negatively charged CNTs (Figure S14 and Table S5). However, the current density for ORR by *Ha*CueO WT on negatively charged CNTs is twice as high as that of *Ec*CueO WT, suggesting a slightly different distribution of surface charges on the enzyme molecules. Indeed, while both enzymes exhibit a similar patch of negatively charged residues near the Cu-T1 site, the charges in *Ha*CueO are distributed more homogeneously across the surface (Figures S15 and S16). The deletion of the bulky Met-rich domains covering the Cu-T1 center facilitates electron transfer for *Ha*CueO ΔMet at CNT-COOH-based electrodes, as evidenced by the increase in the DET-current (Figure 5).

The addition of Cu^{2+} to the electrolyte results in an increase in the electrocatalytic current for both *Ha*CueO enzymes.

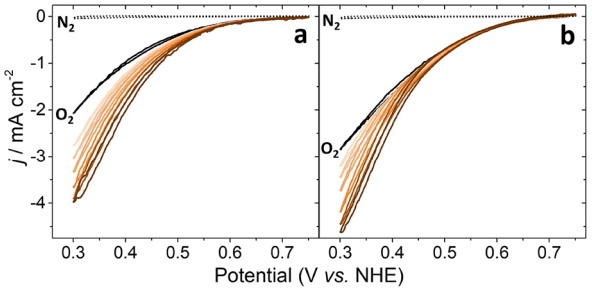

Figure 5. Electrochemical activity of *Ha*CueO: WT (a) and ΔMet (b). Cyclic voltammograms obtained with CueO functionalized COOH-CNT based electrodes under N_2 (black dashed line), O_2 (black line), and O_2 in the presence of increasing $CuSO_4$ concentrations (brown lines). $CuSO_4$ concentrations: 0.05, 0.1, 0.2, 0.5, 1, and 2 mM. Experimental conditions: 100 mM sodium acetate buffer, pH 5.0 at 30 °C, ω = 3000 rpm ν = 5 mV s^{-1}.

https://doi.org/10.1021/jacsau.5c00076
JACS Au 2025, 5, 1833−1844

*Ha*CueO is thus capable of carrying out electrocuprous oxidation as *Ec*CueO (Figure 5).

The quantification of the electrochemical cuprous oxidase activity was done by chronoamperometry. Poising the electrode at a specific potential in the presence of $CuSO_4$ allows generating and maintaining a constant substrate (Cu^+) concentration near the electrode surface, which can be calculated based on known thermodynamic constants.[9] The presence of an active enzyme on the electrode initiates the catalytic cycle, resulting in a rapid increase in the catalytic current (Figure 6A). It is to be noted that the catalytic current for oxygen reduction in the absence of copper is not zero and cannot be neglected. We, therefore, used a modified Michaelis–Menten equation, incorporating this background current as j_0, and j_{max} being the maximal total current density (eq 1):

$$j = j_0 + \frac{(j_{max} - j_0) \times [S]}{K_m + [S]} \quad (1)$$

The measured current density at each concentration of $CuSO_4$ was fitted to the modified Michaelis–Menten equation (Figure 6B). The apparent kinetics parameters for the electrocuprous oxidase activity of CueOs are provided in Table S6 and Figure 6C. Compared to reported data for *Ec*CueOs,[9] the maximum activation of *Ha*CueOs was achieved with a three-fold lower concentration of Cu^+. This resulted in an apparent K_m for Cu^+ in *Ha*CueO WT being lower than that of *Ec*CueO WT (41 ± 4 and 75 ± 19 nM, respectively).

The absence of the Met-rich domain has a minor effect on the electrocuprous oxidase activity. An increase in $_{app}K_m$ is observed, which is likely related to the loss of one Cu5 ligand. However, this increase in $_{app}K_m$ is compensated by an increase of j_{max} due to the shortened distance to the CNTs surface. As a result, the apparent electrocatalytic efficiencies ($j_{max}/_{app}K_m$) remain virtually unchanged upon Met-rich domain deletion. As concluded for *Ec*CueO,[9] we thus confirm that the Met-rich domain is not essential and can be bypassed when Cu^+ is provided in a weakly chelated form, as in this electrochemical experiment. Nevertheless, due to its lower apparent K_m compared to *Ec*CueO, *Ha*CueO proves to be a more efficient cuprous oxidase enzyme, both with and without the Met-rich domain.

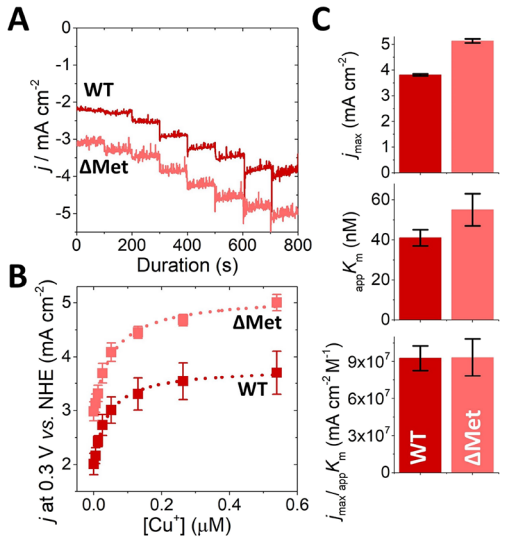

Figure 6. Electrocuprous oxidase activity quantification. (A) Chronoamperometry at 0.3 V vs NHE, under O_2 and increasing concentrations of $CuSO_4$: 0.02, 0.05, 0.1, 0.2, 0.5, 1, and 2 mM for *Ha*CueO WT (red) and *Ha*CueO ΔMet (salmon). (B) Apparent Michaelis–Menten fit of the current density j at 0.3 V vs NHE in the presence of electrogenerated Cu^+ species. (C) Resulting j_{max}, $_{app}K_m$ and $j_{max}/_{app}K_m$ from apparent Michaelis–Menten fit of (B).

In Vitro Ferroxidase Activity of CueOs

CueO is physiologically active in cuprous oxidation, but isolated *Ec*CueO WT has also been reported to exhibit Fe^{2+} oxidase activity, which can be enhanced by the addition of Cu^{2+}.[4] To pursue the investigation of the role of the Met-rich domain on *Ha*CueO activity in the presence of free Cu^{2+}, we have tested *Ha*CueO ferroxidase activity using $(NH_4)_2Fe$-

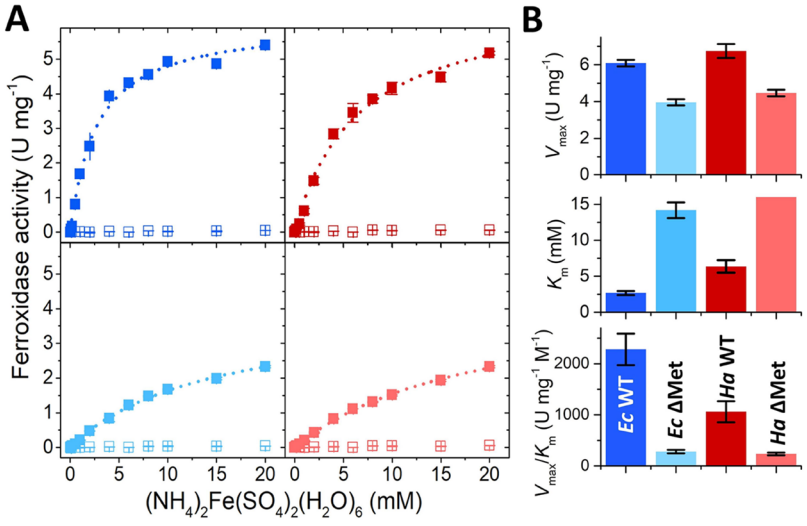

Figure 7. (A) Ferroxidase activity of CueOs: *Ec* WT (a), *Ha* WT (b), *Ec* ΔMet (c), and *Ha* ΔMet (d) in the absence (empty squares) and in the presence of 500 μM $CuSO_4$ (filled squares). Dashed lines represent Michaelis–Menten fit for Fe^{2+} oxidation in the presence of $CuSO_4$. (B) Resulting V_{max}, K_m, and V_{max}/K_m from Michaelis–Menten fits in the presence of 500 μM $CuSO_4$. Columns coloration for CueOs: *Ec* WT (blue), *Ec* ΔMet (cyan), *Ha* WT (red), and *Ha* ΔMet (salmon).

https://doi.org/10.1021/jacsau.5c00076
JACS Au 2025, 5, 1833–1844

$(SO_4)_2(H_2O)_6$ (Mohr's salt)[18] in the absence or presence of 500 μM $CuSO_4$ and compared it to *Ec*CueO tested under the same experimental conditions (Figure 7).

In the absence of Cu^{2+}, WT and ΔMet CueOs demonstrate negligible activity, which is observable only at the highest concentrations of Mohr's salt and cannot be fitted to the Michaelis–Menten eq (Figure 7A). Interestingly, the addition of 500 μM $CuSO_4$ stimulates CueO ferroxidase activity, enabling the estimation of kinetic parameters (Figure 7B and Table S7). Direct oxidation of Fe^{2+} by Cu^{2+} can be ruled out, as no Fe^{3+} formation was observed in the presence of the inactive Cu-T1-depleted *Ec*CueO variant (Figure S17). Removal of the Met-rich domain leads to a several-fold increase in K_m and a 30% decrease in the rate of catalysis for both CueOs.

Such activation upon $CuSO_4$ addition resembles the known enhancement of phenol oxidase activity of CueOs, e.g., when ABTS is used as a substrate (Figure S18 and Table S8).[4,8,9] It was proposed that this activation with ABTS can be explained by Cu^{2+} binding to the Cu5 site, acting as an electron relay for ABTS oxidation.[4,8,9] By similar reasoning, the enhancement of ferrous oxidase activity could likely be attributed to electron transfer from Fe^{2+} to Cu^{2+} bound at the Cu5-site and subsequently to the Cu-T1 and TNC center.

In contrast to Fe^{2+} oxidation, in the case of ABTS oxidation, the removal of the Met-rich domain led to a burst in activity for both *Ha*CueO and *Ec*CueO in the absence of Cu^{2+} (Figure S18 and Table S8).[9] This behavior has been previously explained by the removal of steric hindrance that prevented a bulky substrate like ABTS from approaching the Cu-T1 center. Given the small size of Fe^{2+} and because ΔMet enzymes are as inactive as the WT, the lack of significant ferrous oxidase activity cannot be attributed to steric hindrance induced by the Met-rich domain. Instead, it is more likely due to the absence of a suitable Fe^{2+}-binding site near the Cu-T1 center. The lack of ferrous oxidase activity also suggests that Fe^{2+} does not bind to the Cu5 site, which is highly specific to cuprous oxidation.

Yet, even in the presence of Cu^{2+}, the ferrous oxidase activity of CueOs does not appear to be physiologically relevant, as the observed K_m in the millimolar range far exceeds the intracellular iron concentrations, which are typically in the micromolar range.[19−21] In agreement, MCO enzymes known to catalyze both cuprous and ferrous oxidase activities, such as ceruloplasmin, *Sc*Fet3p, and *Ca*Fet34, display K_m for both substrates in the micromolar range.[22−25] Nevertheless, ferrous oxidase activity is useful for our purposes. First, in the absence of Cu^{2+}, the presence or absence of the Met-rich domain does not affect the almost negligible ferrous oxidase activity. Second, in the presence of Cu^{2+}, both *Ha*CueO WT and *Ec*CueO WT, as well as *Ha*CueO ΔMet and *Ec*CueO ΔMet, exhibit similar behavior and kinetic parameters for ferrous oxidase activity (*Ec*CueO being even more efficient than *Ha*CueO). The decrease in K_m observed with both ΔMet variants compared to WTs in the presence of Cu^{2+} is likely attributable solely to changes in Cu^{2+} binding at the Cu5-site due to D362 deletion. Since the ferrous oxidase activity is unrelated to the Met-rich domain, it supports the equivalence of both enzyme preparations in terms of internal electron transfer chain activity, thereby validating subsequent comparisons.

In Vitro Cu^+ Oxidase Activity of CueOs Using Soluble Cu^+-Complexes

The aforementioned in vivo and in vitro tests revealed either no differences between *Ha*CueO and *Ec*CueO, or only minor differences, which do not seem to be related to the Met-rich domain composition, leading to the question of whether the longer Met-rich domain truly has any functional significance for cuprous oxidation. To address this, we conducted measurements of *Ha*CueOs cuprous oxidation activity in solution using different Cu^+ complexes to mitigate the intrinsic instability of Cu^+ under aerobic conditions. The most widely used Cu^+ complex is $[Cu^I(BCA)_2]^{3-}$,[9,26,27] while other complexes have been used to measure the transfer rate of Cu^+ to copper-binding proteins.[28−32] In our recent study, we demonstrated how the affinity for Cu^+ of the ligand can influence and control the catalytic efficiencies of *Ec*CueO WT and ΔMet.[9] To first confirm the role of the Met-rich domain in copper recruitment from strong chelated forms, we compared the activity of *Ha*CueOs toward $[Cu^I(Ferene)_2]^{3-}$, $[Cu^I(BCA)_2]^{3-}$, and $[Cu^I(BCS)_2]^{3-}$ complexes with log β_2 values of 13.7, 17.2, and 19.8, respectively. Enzymatic oxidation of all tested Cu^+-complexes was observed, resulting in Michaelis–Menten behaviors (Figure 8). Table S9 reports the resulting kinetic parameters for each substrate employed.

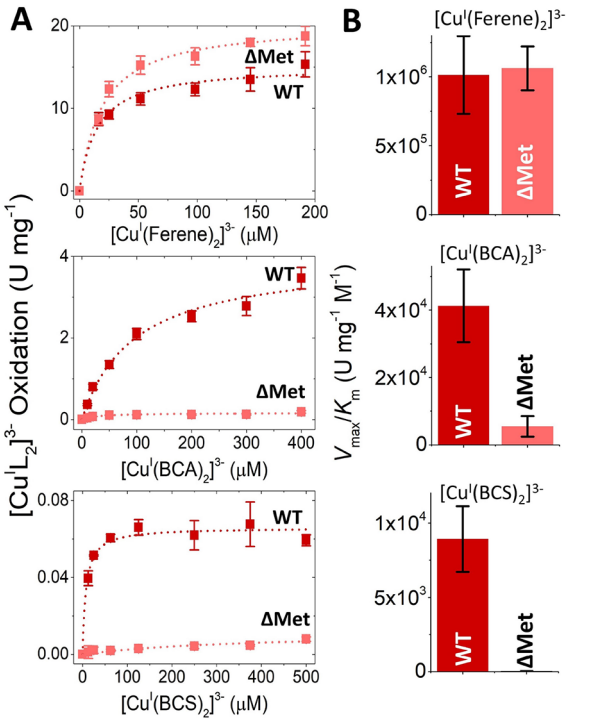

Figure 8. (A) Cuprous oxidase activity of *Ha*CueO: WT (red) and ΔMet (salmon). Dashed lines represent Michaelis–Menten fits for $[Cu^I(L)_2]^{3-}$ oxidation. (B) Catalytic efficiency (V_{max}/K_m) of *Ha*CueOs for $[Cu^I(L)_2]^{3-}$ oxidation.

The catalytic efficiency decreases in the order $[Cu^I(Ferene)_2]^{3-} \rightarrow [Cu^I(BCA)_2]^{3-} \rightarrow [Cu^I(BCS)_2]^{3-}$, thus being inversely proportional to the stability of the substrate complex. Upon loss of the Met-rich domain, decrease to less than 10% and 1% of the respective WT catalytic efficiency is obtained for $[Cu^I(BCA)_2]^{3-}$ and $[Cu^I(BCS)_2]^{3-}$. In contrast, the loss of the Met-rich domain does not impact significantly the catalytic efficiencies of the enzyme with $[Cu^I(Ferene)_2]^{3-}$,

https://doi.org/10.1021/jacsau.5c00076
JACS Au 2025, 5, 1833−1844

the least chelated substrate. These behaviors are very similar to what was reported for *Ec*CueOs, and allow to confirm that the Met-rich domain is not essential for Cu^{+} oxidation and can be bypassed when the substrate is weakly chelated.[9]

One particularity observed with *Ha*CueO WT is that its catalytic efficiencies for all substrates exceed those previously reported for *Ec*CueO WT, regardless of the strength of Cu^{+}-chelation,[9] hinting at a potential importance of the length of the Met-rich domain. To test this hypothesis, we generated conditions where Cu^{+} was sufficiently chelated to highlight the Met-domain's influence, yet not so strongly chelated as to prevent accurate determination of kinetic parameters (Figure S19 and Table S9). This was achieved by finely adjusting Cu^{+}:BCA^{2-} ratio from the least chelating (1:2) to a more strongly chelating one (1:4) (Figure 9). The activity of

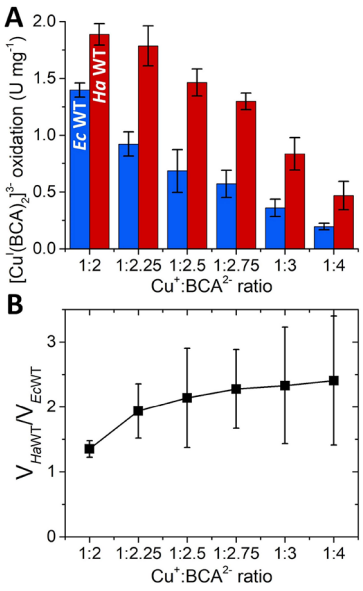

Figure 9. (A) $[Cu^{I}(BCA)_2]^{3-}$ oxidation at the constant concentration of 100 μM for *Ec*CueO WT (blue) and *Ha*CueO WT (red). The Cu^{+}:BCA ratio from 1:2 to 1:4. (B) WT CueO ratio of the rate of $[Cu^{I}(BCA)_2]^{3-}$ oxidation from (A).

*Ha*CueO was compared to that of *Ec*CueO, which possesses a smaller Met-rich domain (Figure 2A). As suggested by Djoko et al., an excess of free BCA^{2-} limits Cu^{+} availability resulting in a lower catalytic rate.[26] Accordingly, the activities of both CueOs decrease as BCA^{2-} excess increases. However, *Ha*CueO WT consistently outperforms *Ec*CueO WT across all BCA^{2-} levels (Figure 9). Furthermore, the activity ratio of *Ha*CueO to *Ec*CueO (Figure 9B) increases as BCA^{2-} excess grows, ranging from 1.3 ± 0.1 (Cu^{+}:BCA^{2-} = 1:2) to 2.4 ± 1.0 (Cu^{+}:BCA^{2-} = 1:4). These data definitely demonstrate that the larger and richer in methionines domain of *Ha*CueO is crucial to enhance cuprous oxidase activity of *Ha*CueO when Cu^{+} is strongly chelated, while its significance diminishes when Cu^{+} is weakly chelated.

CONCLUSIONS

Studying multiple proteins with distinct features within the same family provides valuable insights into the relationship between structure and function. In this study, we identified, isolated, and characterized a novel multicopper oxidase (MCO) from *Hafnia alvei* bacterium containing a domain significantly larger and richer in Met residues compared to the well-known *Ec*CueO. We solved the crystal structure of *Ha*CueO and showed that the MCO structure is conserved, including Cu-T1 and TNC copper sites. The structure also highlighted that the main features of CueO-like proteins are conserved, especially the presence of the Cu5 coordinating site. The unique similarity between *Ha*CueO and *Ec*CueO in terms of overall structure, apart from the Met-rich domain, allowed us to establish a clear structure−function relation between the length of the Met-rich domain and cuprous oxidase activity. MD simulations confirmed the flexible nature of the Met-rich domain, which could not be fully resolved in the crystal structure, but indicated the potential formation of helical secondary structures within it. To investigate the effect of the methionine content and length of the Met-rich domain, we constructed the variant ΔMet where the entire Met-rich domain is absent. We studied the activities of the WT and ΔMet proteins by electrochemistry and in solution and compared them to *Ec*CueOs. *Ha*CueO demonstrated the features of a typical CueO and the ability to oxidize all the tested substrates of *Ec*CueO. Similar to *Ec*CueO, *Ha*CueO does not display ferrous oxidase activity in the absence of Cu^{2+}. Given that the Met-rich domain is not involved in CueO ferroxidase activity and is absent in true MCO ferroxidase enzymes, it can be inferred that the Met-rich domain is specifically associated with cuprous oxidase activity. *Ha*CueO ΔMet variant also showed similar activity to WT when the assay involved weakly chelated Cu^{+} species, such as $[Cu^{I}(Ferene)_2]^{3-}$ complex or electrogenerated Cu^{+}. This confirms our previous conclusion established for *Ec*CueO that the Met-rich domain can be bypassed for such species.[9] Such conditions are probably encountered in our survival assay, explaining the similar behavior of all tested constructs.

When strongly chelating species (BCA^{2-} and BCS^{2-}) were used, *Ha*CueO WT became much more active than ΔMet. Furthermore, with these strongly chelating species, *Ha*CueO WT consistently outperformed *Ec*CueO, with the difference increasing as chelator excess increased. This suggests that the Met-rich domain is required for Cu^{+} recruitment from strongly chelated species and is more efficient in *Ha*CueO than in *Ec*CueO. In addition to its higher methionine content, MD simulations suggest that one of the reasons for this efficiency might be the greater flexibility of the *Ha*CueO domain, allowing it to adopt conformations more favorable for interaction. Biologically, such a large Met-rich domain can therefore confer distinct advantages to *Ha*CueO under conditions of a highly chelated environment or in the recruitment of copper from copper-binding metallophores. From a biotechnological perspective, *Ha*CueO's ability to oxidize Cu^{+} chelated by ligands with stability constants (β) as high as 20 highlights the potential of these proteins for applications as Cu^{+} sensors and Cu^{+}-detoxification in complex environments.

METHODS

Copper Survival Assays

The Δ*cusB* Δ*cueO* MG1655 cells carrying CueO expressing plasmids were grown aerobically at 37 °C under agitation in 10 mL of M9 minimal medium with ampicillin (100 μg/mL) and IPTG (100 μM). When cultures reached $OD_{600\ nm} \approx 0.1$, cells were harvested and diluted in phosphate buffered saline (PBS): 5 μL of 10-time serial dilutions was spotted onto M9 minimal medium-agar plates with

https://doi.org/10.1021/jacsau.5c00076
JACS Au 2025, 5, 1833−1844

Ampicillin (100 μg/mL) and IPTG (100 μM) supplemented or not with $CuSO_4$ (80 μM). Plates were incubated at 37 °C for 3 days.

Expression and Purification of CueOs

CueO expression and purification have been performed as previously described.[9] In brief, CueO-transformed *E. coli* cells were grown in LB Broth (Miller's) with 100 μg mL^{-1} ampicillin at 37 °C up to $OD_{600\ nm}$ 0.6, and 0.1 mM IPTG was then added to induce gene expression. Cultures were supplemented with 0.5 mM $CuSO_4$ and then grown for 24 h at 25 °C. Cells were harvested by centrifugation at 5000 rpm, and the bacteria pellets were resuspended at 4 °C in 50 mM PBS at pH 7.4 containing 1 mM phenylmethylsulfonyl fluoride (PMSF), 10 μg mL^{-1} DNase I and 2 mM $MgSO_4$. Cell lysis was performed using French Press (Thermo Scientific) at 4 °C, 1000 psi two times. The cell debris was removed by ultracentrifugation at 40 krpm for 45 min at 4 °C. The cleared lysate was filtered (cutoff 0.45 μm) prior to being loaded onto Strep-TactinXT 4Flow (IBA Lifesciences) 5 mL column; nonadsorbed proteins were washed with 50 mM PBS at pH 7.4 and 50 mM PBS and 150 mM NaCl at pH 7.4, and *Ha*CueOs were eluted with 50 mM PBS and biotin 5 mM at pH 7.4. Eluted CueOs were concentrated up to 100 μM and desalted with 40 mM MOPS buffer at pH 7.0, using a HiPrep 26/10 Desalting column (Cytiva). An in vitro copper incorporation step was carried out for all CueOs by dialyzing overnight at 4 °C in 40 mM MOPS buffer at pH 7.0 with the addition of 5 equiv of $CuSO_4$. The excess copper was removed by desalting with 40 mM MOPS buffer at pH 7.0, using a HiPrep 26/10 Desalting column (Cytiva). Pure CueO preparations were aliquoted, frozen in liquid nitrogen, and stored at −80 °C. Except for the CueOs that served for the crystallogenesis assays, after the copper incorporation step, the excess of copper and the buffer was exchanged with 20 mM HEPES buffer and 150 mM NaCl at pH 7.0, using a HiLoad 16/600 Superdex 75 pg (Cytiva). The homogeneous samples of CueOs have been concentrated and stored at 4 °C prior to crystallogenesis assays. Crystallogenesis assays were performed within 1 month of protein isolation. During this period and under these conditions, the protein remained stable and retained its blue color and substantial activity in solution and for O_2 electroreduction.

*Ha*CueO WT and ΔMet Crystallization, Structure Determination, and Refinement

The purified CueO WT and ΔMet were concentrated to 38 and 36 mg mL^{-1}, respectively. Crystallization trials were performed using the sitting-drop vapor-diffusion method at 293 K in 96-well Swissci-3 plates, with Stura Footprint (Molecular Dimensions), Wizard I and II (Rigaku), and Structure I and II (Molecular Dimensions) screens, and using Tecan and Mosquito (TTP Labtech) robots to fill in the plates and dispense the drops, respectively. Rod-shaped blue crystals appeared in a number of different conditions after 1 week, but in some conditions, crystals started to lose the blue coloration after 1 month. Therefore, crystals were harvested a few days after they appeared, to ensure sufficient growth while preventing copper depletion. The selected crystallization condition for *Ha*CueO WT was No. A6 from Wizard I screen (0.1 M sodium citrate pH 5.5, 20% PEG 3000) and No. C5 from Stura Footprint #2 screen (0.1 M sodium acetate pH 5.5, 24% PEG 5000 mme) for *Ha*CueO ΔMet. Crystals were mounted in cryo-loops (Hampton CrystalCap Magnetic) and were briefly soaked in crystallization solution supplemented with 20% (v/v) ethylene glycol before being flash-cooled in liquid nitrogen.

*Ha*CueO WT and ΔMet diffraction data were collected at 3.2 and 3.0 Å, respectively, on beamline Proxima-1 at the Soleil synchrotron. The data sets were indexed and integrated using XDS[33] and scaled with SCALA[34] from the CCP4 Suite.[35] The structure of *Ha*CueO WT was solved by molecular replacement with Molrep[36] using the structure of *Ec*CueO WT (PDB entry 1KV7) as the model and was subsequently used as a model to solve the structure of *Ha*CueO ΔMet by molecular replacement with Molrep. Refinement, correction, and validation of the structures were performed with autoBUSTER,[37] COOT,[38] and MolProbity.[39] Data collection and refinement statistics are listed in Table S4.

Molecular Dynamics

The initial structure of full-length *Ha*CueO WT for the simulations was obtained from the AlphaFold3 Server,[40] by providing the protein sequence (excluding the signal peptide and Strep-tag) and specifying four copper atoms. All subsequent processing, simulation, and trajectory analyses were conducted using YASARA software.[41] Simulation preparation included fixing the metal ions to the known coordinating residues using string pseudobonds, optimizing the hydrogen bonding network, and performing a pK_a prediction to assign the protonation states for protein residues at pH 7.4. The protein was positioned in a cubic periodic box with a minimum distance of 10 Å from the box edges, with water molecules modeled using the TIP3P model. Counterions (Na^+ and Cl^-) were added to neutralize the system and mimic a physiological concentration of 0.9%. After steepest descent and simulated annealing minimizations to remove clashes, the simulations were run for 500 ns using the AMBER14 force field,[42] with time step 2.5 fs for bonded and 5.0 fs for nonbonded interactions at a temperature of 298 K and a pressure of 1 atm (*NPT* ensemble). The temperature was controlled by rescaling velocities with a Berendsen thermostat based on the time-averaged temperature, while pressure was maintained by resizing the simulation cell to achieve an average solvent density. To confirm result reproducibility, two additional simulations were carried out from the same starting structure using different random seeds. To compare the average structures from the MD simulations to the crystal structure, the structures were aligned and RMSD of Cα was calculated with the MUSTANG algorithm.[43] The first 10 ns was considered as the equilibration phase and were excluded from all analyses, except for RMSD calculations.

For comparison, three parallel MD simulations were also conducted for *Ec*CueO under the exact same conditions as those used for *Ha*CueO, utilizing its crystallographic structure with a fully resolved Met-rich domain (PDB accession number: 3OD3) as the initial model.

Conformational clustering of the MD trajectory was performed using the RMSD of heavy atoms as a similarity metric. A cutoff value of 3.0 Å (for *Ha*CueO) or 2.5 Å (for *Ec*CueO) RMSD was used to define distinct conformational states and the representative structure of each cluster was extracted.

The dynamic cross-correlation matrix (DCCM) for backbone Cα atoms was computed to assess correlated motions between residues during the MD simulation. Individual matrices from three parallel simulations were averaged to display the DCCM matrix as a heatmap with values from −1 (fully anticorrelated motion) to 1 (fully correlated motion).

Principal component analysis (PCA) was applied to the MD trajectory to identify dominant collective motions of the residues. The covariance matrix of atomic fluctuations was constructed using backbone N, C, and Cα atomic positions, and eigenvector decomposition was performed to obtain principal components. The first three principal components were selected for further analysis and visualization.

Preparation of the CueO-Based COOH-CNT-Functionalized Working Electrodes

CueO bioelectrodes were prepared as previously reported.[8,9] Planar glassy carbon electrodes (GCs; diameter: 3 mm) were polished with an alumina slurry, sonicated for 10 min first in acetone/ethanol 1:1 and then in Milli-Q water, and finally rinsed with Milli-Q water. Then, COOH−CNT slurry dispersed in water was drop cast onto the surface of GCs and dried at 60 °C. A 10 μL aliquot of 15 μM CueO preparation was drop cast on the CNT-based electrode and incubated under the air for 30 min at 4 °C. The enzyme-modified electrode was washed with 40 mM MOPS buffer at pH 7.0 and was stored in the same buffer under air at 4 °C when not used.

Electrochemical Measurements

Electrochemical experiments [cyclic voltammetry (CV) and chronoamperometry (CA)] were carried out in a three-electrode electrochemical cell using Autolab PGSTAT30 potentiostat, con-

https://doi.org/10.1021/jacsau.5c00076
JACS Au 2025, 5, 1833−1844

trolled by Nova software, and a rotating electrode instrument (Metrohm Autolab, Switzerland). The rotation speed (ω) of the working electrode was set to 3000 rpm. The CNT-based bioelectrodes were used as working electrodes. Pt wire was used as a counter electrode and the Hg|Hg_2SO_4|sat. K_2SO_4 served as a reference electrode. Potentials are referred to the Normal Hydrogen Electrode according to $E_{NHE} = E_{MSE} + 0.64$ V. All current densities are normalized toward the geometrical surface of the glassy carbon electrode (0.071 cm^2). The experiments were conducted at 30 °C and under a controlled oxygen or nitrogen-saturated atmosphere, by continuously bubbling either O_2 or N_2 gas in the electrolyte solution. The supporting electrolyte was 100 mM sodium acetate buffer at pH 5.0 for all experiments. Additions of $CuSO_4$ to the electrolyte solution were performed every 100 s for CA; and at the highest potential (0.74 V vs NHE) for CV experiments. For each CueO preparation, at least four bioelectrodes were evaluated for each electrochemical measurement.

Cuprous Oxidase and Ferroxidase Activities of CueOs in Solution

Air-stable substrates $[Cu^I(L)_2]^{3-}$ (L = ferene, BCA, and BCS) were used for measuring the cuprous oxidase activity of CueOs. Stock solutions were prepared as previously reported[9,26]: 1 mM $[Cu^I(BCS)_2]^{3-}$ by dissolving 1 mM $[Cu^I(CH_3CN)_4]PF_6$ in 50 mM BisTris buffer with 2.5 mM bathocuproinedisulfonic acid disodium salt (BCS) at pH 7.0 under anaerobic conditions; 800 μM $[Cu^I(BCA)_2]^{3-}$ by dissolving 800 μM $[Cu^I(CH_3CN)_4]PF_6$ in 50 mM BisTris buffer and 1.6 mM bicinchoninic acid disodium salt hydrate (BCA) at pH 7.0 under anaerobic conditions; and 800 μM $[Cu^I(Ferene)_2]^{3-}$, by dissolving 800 μM $[Cu^I(CH_3CN)_4]PF_6$ in 50 mM BisTris buffer and 4 mM ferene disodium salt (Ferene) at pH 7.0 under anaerobic conditions. The final Cu^+/L ratios were 1/2.5 for $[Cu^I(BCS)_2]^{3-}$, 1/2 for $[Cu^I(BCA)_2]^{3-}$, and 1/5 for $[Cu^I(Ferene)_2]^{3-}$. For the competition test, several $[Cu^I(BCA)_2]^{3-}$ stocks were prepared similarly by mixing 800 μM $[Cu^I(CH_3CN)_4]$-PF_6 in 50 mM BisTris buffer, with 1.8 mM (1/2.25) or 2 mM (1/2.5) or 2.2 mM (1/2.75) or 2.4 mM (1/3) or 3.2 mM (1/4) BCA at pH 7.0 under anaerobic conditions. The $[Cu^I(L)_2]^{3-}$ stock concentration was checked prior to measuring CueO activity and calculated from $\varepsilon_{562\ nm}$ = 7900 M^{-1} cm^{-1} for $[Cu^I(BCA)_2]^{3-}$, $\varepsilon_{482\ nm}$ = 13,300 M^{-1} cm^{-1} for $[Cu^I(BCS)_2]^{3-}$, and $\varepsilon_{484\ nm}$ = 6700 M^{-1} cm^{-1} for $[Cu^I(Ferene)_2]^{3-}$.[26,28,30]

Enzymatic assays were performed under the air at 30 °C by measuring the absorption decrease at 562/484/482 nm using a spectrophotometer microplate reader (Spark 10 M, Tecan, Swiss). To avoid any product inhibition during kinetic measurements, the cuprous oxidase activity was measured in 50 mM BisTris buffer at pH 7.0, selected for its ability to coordinate the excess of Cu^{2+}.[26] Values reported in Table S9, Figures 8 and 9 come from at least 12 measurements for each concentration of substrate and are normalized for substrate auto-oxidation in the absence of enzyme. The CueO enzymatic preparations come from different expressions and purifications. CueO concentrations in the well were: 0.5 ± 0.25 μM for $[Cu^I(BCS)_2]^{3-}$, 0.075 ± 0.025 μM for $[Cu^I(BCA)_2]^{3-}$, and 0.012 ± 0.003 μM for $[Cu^I(Ferene)_2]^{3-}$. The reaction buffer was composed of 50 mM BisTris at pH 7.0 with increasing concentrations of $[Cu^I(L)_2]^{3-}$.

$[Cu^I(L)_2]^{3-}$ kinetic parameters of CueOs were calculated by OriginPro 2016 (OriginLab Corporation, Massachussetts, USA), using the first 600, 200, and 100 s to make a linear fit and estimate the reaction rate, respectively for $[Cu^I(BCS)_2]^{3-}$, $[Cu^I(BCA)_2]^{3-}$, and $[Cu^I(Ferene)_2]^{3-}$. The resulting reaction rates were fitted with the Michaelis–Menten equation with one site saturation: $V_i = (V_{max} \times [S]_0)/(K_m + [S]_0)$. Where V_i = initial speed, V_{max} = maximal initial speed, K_m = Michaelis constant, and $[S]_0$ = $[Cu^I(L)_2]^{3-}$ concentration.

$(NH_4)_2Fe(SO_4)_2(H_2O)_6$ (Mohr's salt) was used as an electron donor for measuring the ferroxidase activity of CueOs. Enzymatic assays were performed as mentioned above, except the wavelength of absorption at 415 nm, which allows following Fe^{3+} formation. The reaction buffer was composed of 100 mM sodium acetate at pH 5.0 with increasing concentrations of Mohr's salt from 0 to 20 mM. Ferroxidase kinetic parameters of CueOs were calculated by OriginPro 2016 (OriginLab Corporation, Massachusetts, USA), using the first 250 s to make a linear fit and estimate the reaction rate. The resulting reaction rates were fitted with the Michaelis–Menten equation with one site saturation as mentioned above. The Michaelis–Menten fit for the activity in the absence of 0.5 mM $CuSO_4$ was not reliable, suggesting an average K_m of about 400 mM Mohr's salt.

■ ASSOCIATED CONTENT

Supporting Information

The Supporting Information is available free of charge at https://pubs.acs.org/doi/10.1021/jacsau.5c00076.

Chemical and materials, plasmid construction, *Ha*cueO ΔMet construction, size-exclusion chromatography, circular dichroism spectroscopy, UV–visible absorption spectra, copper content determination using ICP-OES, EPR spectroscopy, protein modeling, preparation of the CueO functionalized NH_2-CNT-based working electrodes and in vitro ABTS oxidase activities of *Ha*CueOs (PDF)

MD trajectories of three parallel runs of *Ha*CueO WT (AVI)

Dominant motions of *Ha*CueO, as captured by the first three principal components, while keeping all other components fixed (AVI)

■ AUTHOR INFORMATION

Corresponding Authors

Umberto Contaldo − *CNRS, Laboratoire de Bioénergétique et Ingénierie des Protéines (BIP), Institut de Microbiologie de la Méditerranée, Aix Marseille Université, 13402 Marseille, France;* orcid.org/0000-0002-1700-170X; Email: ucontaldo@imm.cnrs.fr

Elisabeth Lojou − *CNRS, Laboratoire de Bioénergétique et Ingénierie des Protéines (BIP), Institut de Microbiologie de la Méditerranée, Aix Marseille Université, 13402 Marseille, France;* orcid.org/0000-0003-2593-4670; Email: lojou@imm.cnrs.fr

Ievgen Mazurenko − *CNRS, Laboratoire de Bioénergétique et Ingénierie des Protéines (BIP), Institut de Microbiologie de la Méditerranée, Aix Marseille Université, 13402 Marseille, France;* orcid.org/0000-0003-2563-3130; Email: imazurenko@imm.cnrs.fr

Authors

Paolo Santucci − *CNRS, Laboratoire de Bioénergétique et Ingénierie des Protéines (BIP), Institut de Microbiologie de la Méditerranée, Aix Marseille Université, 13402 Marseille, France;* orcid.org/0009-0008-1933-4031

Alexandra Vergnes − *CNRS, Laboratoire de Chimie Bactérienne (LCB), Institut de Microbiologie de la Méditerranée, Aix Marseille Université, 13402 Marseille, France*

Philippe Leone − *CNRS, Laboratoire d'Ingénierie des Systèmes Macromoléculaires (LISM), Institut de Microbiologie de la Méditerranée, Aix Marseille Université, 13402 Marseille, France;* orcid.org/0000-0003-0425-5775

https://doi.org/10.1021/jacsau.5c00076
JACS Au 2025, 5, 1833−1844

Jérôme Becam − *CNRS, Laboratoire de Chimie Bactérienne (LCB), Institut de Microbiologie de la Méditerranée, Aix Marseille Université, 13402 Marseille, France*
Frédéric Biaso − *CNRS, Laboratoire de Bioénergétique et Ingénierie des Protéines (BIP), Institut de Microbiologie de la Méditerranée, Aix Marseille Université, 13402 Marseille, France*
Marianne Ilbert − *CNRS, Laboratoire de Bioénergétique et Ingénierie des Protéines (BIP), Institut de Microbiologie de la Méditerranée, Aix Marseille Université, 13402 Marseille, France;* orcid.org/0000-0002-9070-2334
Benjamin Ezraty − *CNRS, Laboratoire de Chimie Bactérienne (LCB), Institut de Microbiologie de la Méditerranée, Aix Marseille Université, 13402 Marseille, France*

Complete contact information is available at: https://pubs.acs.org/10.1021/jacsau.5c00076

Author Contributions

The manuscript was written through contribution of all authors. All authors have given approval to the final version of the manuscript. U.C., B.E., E.L., and I.M. designed research; U.C., P.S., A.V., P.L., I.M., J.B., F.B., and M.I. performed research; U.C., P.S., P.L., I.M., B.E., F.B., and M.I. analyzed data; and U.C., E.L., and I.M. wrote the paper.

Notes

The authors declare no competing financial interest.

■ ACKNOWLEDGMENTS

This work was supported by the National Research Agency (ANR, France) under the grants MetCop (ANR-21-CE44-0024) and ChapCop (ANR-19-CE44-0018). We are grateful to the EPR-MRS facilities of Aix-Marseille University EPR center and the French research infrastructure INFRANALYTICS (FR2054). We thank Veronique Zamboni and the platform of integrative structural biology of Marseille (PBSIM and AFMB) for the assistance with crystallization assays. We are grateful to the staff of the Soleil synchrotron for their assistance and for beamline allocation. We also thank Dylan Savant-Aira (BIP, France) and Laurent Aussel (LCB, France) for the preliminary biochemical tests, as well as Anne de Poulpiquet (BIP, France), Sarah Hostachy, and Pascale Delangle (SYMMES, CEA, France) for the valuable discussions.

■ REFERENCES

(1) Macomber, L.; Imlay, J. A. The Iron-Sulfur Clusters of Dehydratases Are Primary Intracellular Targets of Copper Toxicity. *Proc. Natl. Acad. Sci. U. S. A.* **2009**, *106* (20), 8344−8349.
(2) Zuily, L.; Lahrach, N.; Fassler, R.; Genest, O.; Faller, P.; Sénèque, O.; Denis, Y.; Castanié-Cornet, M.-P.; Genevaux, P.; Jakob, U.; Reichmann, D.; Giudici-Orticoni, M.-T.; Ilbert, M. Copper Induces Protein Aggregation, a Toxic Process Compensated by Molecular Chaperones. *mBio* **2022**, *13* (2), No. e0325121.
(3) Singh, S. K.; Roberts, S. A.; McDevitt, S. F.; Weichsel, A.; Wildner, G. F.; Grass, G. B.; Rensing, C.; Montfort, W. R. Crystal Structures of Multicopper Oxidase CueO Bound to Copper(I) and Silver(I). *J. Biol. Chem.* **2011**, *286* (43), 37849−37857.
(4) Kataoka, K.; Komori, H.; Ueki, Y.; Konno, Y.; Kamitaka, Y.; Kurose, S.; Tsujimura, S.; Higuchi, Y.; Kano, K.; Seo, D.; Sakurai, T. Structure and Function of the Engineered Multicopper Oxidase CueO from Escherichia Coli—Deletion of the Methionine-Rich Helical Region Covering the Substrate-Binding Site. *J. Mol. Biol.* **2007**, *373* (1), 141−152.
(5) Cui, H.; Zhang, L.; Söder, D.; Tang, X.; Davari, M. D.; Schwaneberg, U. Rapid and Oriented Immobilization of Laccases on Electrodes via a Methionine-Rich Peptide. *ACS Catal.* **2021**, *11* (4), 2445−2453.
(6) Adachi, T.; Mazurenko, I.; Mano, N.; Kitazumi, Y.; Kataoka, K.; Kano, K.; Sowa, K.; Lojou, E. Kinetic and Thermodynamic Analysis of Cu2+-Dependent Reductive Inactivation in Direct Electron Transfer-Type Bioelectrocatalysis by Copper Efflux Oxidase. *Electrochim. Acta* **2022**, *429*, No. 140987.
(7) Clément, R.; Wang, X.; Biaso, F.; Ilbert, M.; Mazurenko, I.; Lojou, E. Mutations in the Coordination Spheres of T1 Cu Affect Cu2+-Activation of the Laccase from Thermus Thermophilus. *Biochimie* **2021**, *182*, 228−237.
(8) Hitaishi, V. P.; Clément, R.; Quattrocchi, L.; Parent, P.; Duché, D.; Zuily, L.; Ilbert, M.; Lojou, E.; Mazurenko, I. Interplay between Orientation at Electrodes and Copper Activation of *Thermus Thermophilus* Laccase for O_2 Reduction. *J. Am. Chem. Soc.* **2020**, *142* (3), 1394−1405.
(9) Contaldo, U.; Savant-Aira, D.; Vergnes, A.; Becam, J.; Biaso, F.; Ilbert, M.; Aussel, L.; Ezraty, B.; Lojou, E.; Mazurenko, I. Methionine-Rich Domains Emerge as Facilitators of Copper Recruitment in Detoxification Systems. *Proc. Natl. Acad. Sci. U. S. A.* **2024**, *121* (42), No. e2402862121.
(10) Gräff, M.; Buchholz, P. C. F.; Le Roes-Hill, M.; Pleiss, J. Multicopper Oxidases: Modular Structure, Sequence Space, and Evolutionary Relationships. *Proteins Struct. Funct. Bioinforma.* **2020**, *88* (10), 1329−1339.
(11) Mazurenko, I.; Adachi, T.; Ezraty, B.; Ilbert, M.; Sowa, K.; Lojou, E. Electrochemistry of Copper Efflux Oxidase-like Multicopper Oxidases Involved in Copper Homeostasis. *Curr. Opin. Electrochem.* **2022**, *32*, No. 100919.
(12) Roulling, F.; Godin, A.; Feller, G. Function and Versatile Location of Met-Rich Inserts in Blue Oxidases Involved in Bacterial Copper Resistance. *Biochimie* **2022**, *194*, 118−126.
(13) Li, X.; Wei, Z.; Zhang, M.; Peng, X.; Yu, G.; Teng, M.; Gong, W. Crystal Structures of E. Coli Laccase CueO at Different Copper Concentrations. *Biochem. Biophys. Res. Commun.* **2007**, *354* (1), 21−26.
(14) Durão, P.; Chen, Z.; Fernandes, A. T.; Hildebrandt, P.; Murgida, D. H.; Todorovic, S.; Pereira, M. M.; Melo, E. P.; Martins, L. O. Copper Incorporation into Recombinant CotA Laccase from Bacillus Subtilis: Characterization of Fully Copper Loaded Enzymes. *JBIC J. Biol. Inorg. Chem.* **2008**, *13* (2), 183−193.
(15) Granja-Travez, R. S.; Wilkinson, R. C.; Persinoti, G. F.; Squina, F. M.; Fülöp, V.; Bugg, T. D. H. Structural and Functional Characterisation of Multi-copper Oxidase CueO from Lignin-degrading Bacterium *Ochrobactrum* Sp. Reveal Its Activity towards Lignin Model Compounds and Lignosulfonate. *FEBS J.* **2018**, *285* (9), 1684−1700.
(16) Wang, H.; Liu, X.; Zhao, J.; Yue, Q.; Yan, Y.; Gao, Z.; Dong, Y.; Zhang, Z.; Fan, Y.; Tian, J.; Wu, N.; Gong, Y. Crystal Structures of Multicopper Oxidase CueO G304K Mutant: Structural Basis of the Increased Laccase Activity. *Sci. Rep.* **2018**, *8* (1), 14252.
(17) Borges, P. T.; Brissos, V.; Hernandez, G.; Masgrau, L.; Lucas, M. F.; Monza, E.; Frazão, C.; Cordeiro, T. N.; Martins, L. O. Methionine-Rich Loop of Multicopper Oxidase McoA Follows Open-to-Close Transitions with a Role in Enzyme Catalysis. *ACS Catal.* **2020**, *10* (13), 7162−7176.
(18) Neşelioğlu, S.; Fırat Oğuz, E.; Erel, Ö. Development of a New Colorimetric, Kinetic and Automated Ceruloplasmin Ferroxidase Activity Measurement Method. *Antioxidants* **2022**, *11* (11), 2187.
(19) Braun, V.; Killmann, H. Bacterial Solutions to the Iron-Supply Problem. *Trends Biochem. Sci.* **1999**, *24* (3), 104−109.
(20) Schalk, I. J. Bacterial Siderophores: Diversity, Uptake Pathways and Applications. *Nat. Rev. Microbiol.* **2025**, *23* (1), 24−40.
(21) Golden, M. M.; Heppe, A. C.; Zaremba, C. L.; Wuest, W. M. Metal Chelation as an Antibacterial Strategy for *Pseudomonas Aeruginosa* and *Acinetobacter Baumannii*. *RSC Chem. Biol.* **2024**, *5* (11), 1083−1096.

(22) Stoj, C.; Kosman, D. J. Cuprous Oxidase Activity of Yeast Fet3p and Human Ceruloplasmin: Implication for Function. *FEBS Lett.* **2003**, *554* (3), 422−426.
(23) de Silva, D.; Davis-Kaplan, S.; Fergestad, J.; Kaplan, J. Purification and Characterization of Fet3 Protein, a Yeast Homologue of Ceruloplasmin. *J. Biol. Chem.* **1997**, *272* (22), 14208−14213.
(24) Stoj, C. S.; Augustine, A. J.; Zeigler, L.; Solomon, E. I.; Kosman, D. J. Structural Basis of the Ferrous Iron Specificity of the Yeast Ferroxidase, Fet3p. *Biochemistry* **2006**, *45* (42), 12741−12749.
(25) Ziegler, L.; Terzulli, A.; Gaur, R.; McCarthy, R.; Kosman, D. J. Functional Characterization of the Ferroxidase, Permease High-affinity Iron Transport Complex from *Candida Albicans*. *Mol. Microbiol.* **2011**, *81* (2), 473−485.
(26) Djoko, K. Y.; Chong, L. X.; Wedd, A. G.; Xiao, Z. Reaction Mechanisms of the Multicopper Oxidase CueO from *Escherichia Coli* Support Its Functional Role as a Cuprous Oxidase. *J. Am. Chem. Soc.* **2010**, *132* (6), 2005−2015.
(27) Cortes, L.; Wedd, A. G.; Xiao, Z. The Functional Roles of the Three Copper Sites Associated with the Methionine-Rich Insert in the Multicopper Oxidase CueO from *E. Coli*. *Metallomics* **2015**, *7* (5), 776−785.
(28) Xiao, Z.; Loughlin, F.; George, G. N.; Howlett, G. J.; Wedd, A. G. C-Terminal Domain of the Membrane Copper Transporter Ctr1 from *Saccharomyces Cerevisiae* Binds Four Cu(I) Ions as a Cuprous-Thiolate Polynuclear Cluster: Sub-Femtomolar Cu(I) Affinity of Three Proteins Involved in Copper Trafficking. *J. Am. Chem. Soc.* **2004**, *126* (10), 3081−3090.
(29) Bagchi, P.; Morgan, M. T.; Bacsa, J.; Fahrni, C. J. Robust Affinity Standards for Cu(I) Biochemistry. *J. Am. Chem. Soc.* **2013**, *135* (49), 18549−18559.
(30) Young, T. R.; Wedd, A. G.; Xiao, Z. Evaluation of Cu(i) Binding to the E2 Domain of the Amyloid Precursor Protein−a Lesson in Quantification of Metal Binding to Proteins *via* Ligand Competition. *Metallomics* **2018**, *10* (1), 108−119.
(31) Xiao, Z.; Brose, J.; Schimo, S.; Ackland, S. M.; La Fontaine, S.; Wedd, A. G. Unification of the Copper(I) Binding Affinities of the Metallo-Chaperones Atx1, Atox1, and Related Proteins. *J. Biol. Chem.* **2011**, *286* (13), 11047−11055.
(32) Xiao, Z.; Wedd, A. G. The Challenges of Determining Metal−Protein Affinities. *Nat. Prod. Rep.* **2010**, *27* (5), 768.
(33) Kabsch, W. XDS. *Acta Crystallogr. D Biol. Crystallogr.* **2010**, *66* (2), 125−132.
(34) Evans, P. R. An Introduction to Data Reduction: Space-Group Determination, Scaling and Intensity Statistics. *Acta Crystallogr. D Biol. Crystallogr.* **2011**, *67* (4), 282−292.
(35) Winn, M. D.; Ballard, C. C.; Cowtan, K. D.; Dodson, E. J.; Emsley, P.; Evans, P. R.; Keegan, R. M.; Krissinel, E. B.; Leslie, A. G. W.; McCoy, A.; McNicholas, S. J.; Murshudov, G. N.; Pannu, N. S.; Potterton, E. A.; Powell, H. R.; Read, R. J.; Vagin, A.; Wilson, K. S. Overview of the *CCP*4 Suite and Current Developments. *Acta Crystallogr. D Biol. Crystallogr.* **2011**, *67* (4), 235−242.
(36) Vagin, A.; Teplyakov, A. Molecular Replacement with *MOLREP*. *Acta Crystallogr. D Biol. Crystallogr.* **2010**, *66* (1), 22−25.
(37) Blanc, E.; Roversi, P.; Vonrhein, C.; Flensburg, C.; Lea, S. M.; Bricogne, G. Refinement of Severely Incomplete Structures with Maximum Likelihood in *BUSTER*−*TNT*. *Acta Crystallogr. D Biol. Crystallogr.* **2004**, *60* (12), 2210−2221.
(38) Emsley, P.; Cowtan, K. *Coot*: Model-Building Tools for Molecular Graphics. *Acta Crystallogr. D Biol. Crystallogr.* **2004**, *60* (12), 2126−2132.
(39) Williams, C. J.; Headd, J. J.; Moriarty, N. W.; Prisant, M. G.; Videau, L. L.; Deis, L. N.; Verma, V.; Keedy, D. A.; Hintze, B. J.; Chen, V. B.; Jain, S.; Lewis, S. M.; Arendall, W. B.; Snoeyink, J.; Adams, P. D.; Lovell, S. C.; Richardson, J. S.; Richardson, D. C. MolProbity: More and Better Reference Data for Improved All-atom Structure Validation. *Protein Sci.* **2018**, *27* (1), 293−315.
(40) Abramson, J.; Adler, J.; Dunger, J.; Evans, R.; Green, T.; Pritzel, A.; Ronneberger, O.; Willmore, L.; Ballard, A. J.; Bambrick, J.; Bodenstein, S. W.; Evans, D. A.; Hung, C.-C.; O'Neill, M.; Reiman, D.; Tunyasuvunakool, K.; Wu, Z.; Žemgulytė, A.; Arvaniti, E.; Beattie, C.; Bertolli, O.; Bridgland, A.; Cherepanov, A.; Congreve, M.; Cowen-Rivers, A. I.; Cowie, A.; Figurnov, M.; Fuchs, F. B.; Gladman, H.; Jain, R.; Khan, Y. A.; Low, C. M. R.; Perlin, K.; Potapenko, A.; Savy, P.; Singh, S.; Stecula, A.; Thillaisundaram, A.; Tong, C.; Yakneen, S.; Zhong, E. D.; Zielinski, M.; Žídek, A.; Bapst, V.; Kohli, P.; Jaderberg, M.; Hassabis, D.; Jumper, J. M. Accurate Structure Prediction of Biomolecular Interactions with AlphaFold 3. *Nature* **2024**, *630* (8016), 493−500.
(41) Krieger, E.; Vriend, G. New Ways to Boost Molecular Dynamics Simulations. *J. Comput. Chem.* **2015**, *36* (13), 996−1007.
(42) Maier, J. A.; Martinez, C.; Kasavajhala, K.; Wickstrom, L.; Hauser, K. E.; Simmerling, C. ff14SB: Improving the Accuracy of Protein Side Chain and Backbone Parameters from ff99SB. *J. Chem. Theory Comput.* **2015**, *11* (8), 3696−3713.
(43) Konagurthu, A. S.; Whisstock, J. C.; Stuckey, P. J.; Lesk, A. M. MUSTANG: A Multiple Structural Alignment Algorithm. *Proteins Struct. Funct. Bioinforma.* **2006**, *64* (3), 559−574.

https://doi.org/10.1021/jacsau.5c00076
JACS Au 2025, 5, 1833−1844